Photodiagnosis and Photodynamic Therapy 25 (2019) 492–498

Contents lists available at ScienceDirect

Photodiagnosis and Photodynamic Therapy

journal homepage: www.elsevier.com/locate/pdpdt

Monitoring photodynamic oxygen consumption by endogenous oxygen contrast MRI

Łukasz Ożóg[a], Wojciech Domka[b], Adrian Truszkiewicz[c], Jacek Tarbarkiewicz[a,d], David Aebisher[e,*]

[a] Center for Innovative Research in Medical and Natural Sciences, University of Rzeszów, Warzywna 1A, 35-959, Rzeszów, Poland
[b] Department of Otorhinolaryngology, Frederic Chopin Clinical Hospital No 1 in Rzeszów, Chopin 1, 35-057, Rzeszów, Poland
[c] Institute of Nursing and Health Sciences, Faculty of Medicine, University of Rzeszów, Aleja Rejtana 16A, 35-310, Rzeszów, Poland
[d] Department of Human Immunology, Faculty of Medicine, University of Rzeszów, Aleja Rejtana 16A, 35-310, Rzeszów, Poland
[e] Department of Photomedicine and Physical Chemistry, Faculty of Medicine, University of Rzeszów, Aleja Rejtana 16A, 35-310, Rzeszów, Poland

ARTICLE INFO

Keywords:
Photodynamic action
Singlet oxygen
Magnetic resonance imaging
Endogenous oxygen contrast
Spin-lattice relaxation time

ABSTRACT

Photodynamic oxygen consumption was measured by changes in spin-lattice relaxation time (T_1) in aqueous solution in a clinical GE scanner at 1.5 T. Similar measurements were attempted in excised laryngeal and thyroid tissues that were infused with Rose Bengal. First, T_1 was measured as a function of dissolved oxygen in argon and in oxygen pre-saturated water samples that were opened to the atmosphere in a series of steps allowing air to diffuse into or out of solution; for both argon and oxygen saturated water solutions, stepwise air re-equilibration resulted in a return to air-saturated water T_1. Secondly, T_1 was measured as a function of time under type II photooxidative conditions in aqueous solution. Under type II photooxidative conditions, a 492 ± 53 ms increase in T_1 was measured following 300 s of visible light illumination of aqueous solutions containing the photosensitizer Rose Bengal (2.5×10^{-6} M) and the singlet oxygen trap methionine (0.0012 M). The 492 ± 53 ms increase in T_1 corresponded to consumption of all the measurable dissolved oxygen (~ 0.1 mg O_2 in 15.0 mL of H_2O) during photooxidation of methionine in air saturated water. This rapid oxygen consumption, indicated by an increase in T_1, is due to irreversible trapping of photogenerated singlet oxygen by methionine. Thirdly, an increase in T_1 was observed in Rose Bengal infused normal laryngeal tissue, and in normal and cancerous thyroid tissue samples following 20 min of exposure to visible light. An increase in T_1 was not observed after 40 min of illumination which suggests that the increases in T_1 observed after 20 min were not due to water uptake, but rather to photoconsumption of interstitial dissolved oxygen.

1. Introduction

Photodynamic therapy (PDT) utilizes clinically approved photosensitizers (PS), ground state oxygen ($^3O_2$) and visible light to treat age-related macular degeneration, and cancers of the skin, esophagus, head and neck, lung, and bladder by local photosensitized generation of cytotoxic reactive oxygen species (ROS) [1–3]. In addition, PDT can be utilized to inactivate pathogenic microorganisms [4] and to treat viral infections [5]. Under type II conditions (^3PS-$^3O_2$ energy transfer), singlet oxygen ($^1O_2$) is generated predominantly along with secondary background ROS that are produced due to the presence of minor competing type I electron transfer and hydrogen abstraction channels [6,7]. The process of type II photosensitized generation of $^1O_2$ and ensuing photooxidation of substrates (or in the case of PDT, photooxidative tissue damage) is termed photodynamic action during which available $^3O_2$ is rapidly consumed [7]. As photodynamic action is an oxygen dependent process, tissue hypoxia is a limiting factor in PDT disease treatment [8]. Monitoring changes in oxygen concentration during photodynamic action in tissue by MRI has potential for fine-tuning PDT in regard to estimating tissue hypoxia for singlet oxygen dosimetry. This study was undertaken to assess the feasibility of monitoring oxygen photoconsumption using dissolved oxygen itself as an endogenous MRI contrast agent prior to and following *in vitro* photodynamic action.

Efforts to measure changes in tissue oxygen concentration have included use of microelectrodes [9,10], oxygen dependent phosphorescence and fluorescence quenching [11], and magnetic resonance imaging (MRI), in particular, use of proton spin-lattice relaxation time (T_1), spin-spin relaxation time (T_2), T_2-weighted blood oxygen level dependent

* Corresponding author.
E-mail address: daebisher@ur.edu.pl (D. Aebisher).

https://doi.org/10.1016/j.pdpdt.2019.02.007
Received 2 December 2018; Received in revised form 20 January 2019; Accepted 4 February 2019
Available online 07 February 2019

(BOLD) and T_1 based tissue oxygenation level dependent (TOLD) MRI contrast [12]. In this study, changes in oxygen concentration following photodynamic action in solution and excised tissue were assessed by direct measurements of dissolved oxygen-dependent T_1.

The decrease in proton spin-lattice relaxation time (T_1) and in the spin-spin relaxation time (T_2) of water protons due to the presence of paramagnetic oxygen is well known, and this dependence is attributed mainly to dipole-dipole interactions between dissolved oxygen and water [13–18]. In 1965, Hauser and Noack derived a linear function between the longitudinal relaxation rate of water ($R_1 = 1/T_1$) and the concentration of dissolved oxygen at room temperature [15]. Similar values were reported by Krynicki in 1966 who measured spin-lattice relaxation time in oxygen-free water as a function of temperature (from 0 °C to 100 °C) [13]. Measurements of hypoxia and hyperoxia in fluids and tissue including tumors have been performed using direct T_1 [19,20], BOLD [21,22], and TOLD MRI contrast [23–30]. Blood oxygen level dependent contrast MRI detects decreases in oxygen levels in blood by measuring a decrease in the spin-spin relaxation time (T_2) (or an increase in the transverse relaxation rate $R_2 = 1/T_2$) caused by an increase in paramagnetic deoxyhemoglobin whereas TOLD MRI detects an increase in spin-lattice relaxation time (T_1) (or a decrease in R_1) due to the consumption of paramagnetic oxygen [12].

To the best of our knowledge, the use of endogenous oxygen contrast MRI to estimate the fraction of oxygen consumed as a result of deliberate $^1O_2$ production and trapping has not been explicitly explored, although studies have reported water proton T_1 and T_2 measurements prior to, and after applied PDT [22,32–40], and recently Tain et al. reported decreases in T_1 relaxation time due to induced generation of ROS in egg white treated with hydrogen peroxide [31]. Significant and prolonged increases in T_1 have been reported during irradiation of Photofrin II treated RIF-1 tumors in mice, with smaller increases in T_2 being observed [32]. Comparatively smaller increases in T_2 have also been reported in silicon phthalocyanine (Pc-4) treated murine models of human prostate tumors after irradiation where a pre-PDT value of $T_2 = 55.8 \pm 6.6$ milliseconds increased to a post-PDT value of $T_2 = 68.2 \pm 8.5$ ms [36]. Comparatively larger T_1 times observed after PDT have been ascribed to increases in free water flow into the interstitial tumor space following cell necrosis [32], and changes in T_1 due to cellular and interstitial free water diffusion has been used to distinguish healthy and cancerous tissue [34]. Diffusion-weighted magnetic resonance imaging (DW-MRI) has been used extensively to assess PDT tumor damage by measuring differences in water diffusion in tissue [33–35,39,40]. Spin-lattice relaxation can also aid in distinguishing healthy and cancerous tissue prior to treatment. Damadian reported differences in T_1 between air saturated distilled water and several samples of tissue that follow a decreasing trend e.g. distilled water (T_1, 2.677 s) < hepatoma (T_1, 0.826 s) < normal liver (T_1, 0.293 s) [41]; this trend was ascribed to a higher level of ordering of cellular water within healthy tissue as compared to cancerous tissue and distilled water.

The lifetime of $^1O_2$ is 3.1 μs in water and when generated decomposes back to $^3O_2$ through physical and chemical quenching processes or reacts with substrates yielding oxidized products [42]. The lifetime of singlet oxygen in a single cell has been reported to be on the order of 0.01 - 0.04 μs [43] and more recently estimated to be as long as 3 μs [44]. As $^1O_2$ is physically or chemically quenched to $^3O_2$, the process is repeated via ^{3}PS-$^3O_2$ collision and energy transfer. Ultimately, in an illuminated closed vessel containing PS, all available $^3O_2$ will be consumed by chemical reaction with substrate assuming the concentration of substrate is greater than the concentration of dissolved oxygen and that the PS does not significantly bleach during illumination. We reasoned that illumination of water or tissue-in-water *in vitro* samples containing PS that are kept in air-tight vessels that prevent atmospheric $^3O_2$ replenishment, the fraction of oxygen photoconsumed during photodynamic action could be measured by oxygen-induced changes in T_1.

2. Materials and methods

2.1. Chemicals

DL-methionine (≥ 99%), Rose Bengal disodium salt (95%), sodium nitrite ($NaNO_2$, ACS reagent, ≥ 97%), and deuterium oxide (D_2O, 99.9 atom %D) were purchased from Sigma-Aldrich and used as received. Argon (99%) and oxygen (99%) gas were purchased from STP&DIN Chemicals, Bielsko-Biała, Poland. Water was purified with a AquaB Duo reverse osmosis water treatment system, Fresenius Medical Care, Singapore Pte. Ltd prior to use.

2.2. Excised tissue

Freshly excised samples of normal and cancerous laryngeal tissue and normal and cancerous thyroid tissue were obtained from the Frederic Chopin Clinical Regional Hospital No. 1 in Rzeszów, Poland. The human tissue studies were approved by the Bioethical Commission of the District Medical Chamber in Rzeszów (Resolution number 105/B/2017). Once received, the tissues were stored in 15 mL of deionized water in 15 mL polypropylene graduated conical test tubes fitted with a screw tight cap (Kartell Labware, Milano, Italy) at 5 °C.

2.3. Temperature, pH and dissolved oxygen measurements

Temperature, pH and concentration of dissolved oxygen (in ppm) were measured with an Elmetron multimode CPR-411 probe (Elmetron, Zabrze, Poland).

2.4. Magnetic resonance imaging and nuclear magnetic resonance

Measurement of spin-lattice relaxation time, T_1, was performed using a 1.5 T (T) Magnetic Resonance Imager Optima MR360 Advance from General Electric Healthcare (Milwaukee, Wisconsin, USA). The apparatus was operated under software version SV23. All samples were scanned using Fast Spin-Echo (FSE) sequences with an axial projection using a 4 channel small flex coil. Images were created using a matrix size of 320 × 224, and a field of view (FOV) of 10 cm × 10 cm and a slice thickness of 1 mm. For T_1 measurements, repetition time (TR) values in a range of 50–15,000 ms were used with an echo time (TE) of 3 ms. Based on these values, a pulse sequence was created and the MR image was generated for each sample. Software protocol for determining time T_1 consisted of the following steps: Calibration, 3-Plane, Axial T_1 FSE. In addition, T_2-weighted images were taken.

Postprocessing was done using the GE Advantage Workstation (AW_4.7). For tissue samples, regions of interest (ROIs) were hand-drawn and positioned within each sample in a similar manner. The first ROI, herein termed superficial, represents a surface volume of tissue 1 mm thick in the case of normal and cancerous laryngeal tissue and 2 mm in normal and cancerous thyroid tissue. The second ROI, termed deep, is the inner portion of tissue. Hand drawn superficial and deep ROI is shown for a sample of thyroid neoplasm in Fig. 4b. Separate superficial and deep ROI were chosen to determine potential differences in T_1 due to tissue water and dissolved oxygen. The averaged measured signal intensity for each tissue and aqueous sample for each series of images was used to calculate T_1 relaxation time. T_1 relaxation time values were calculated using non-linear curve adjustments describing the MR signal build-up. In tissue samples, superficial and deep ROI T_1 was reported as an average of 4 separate slice T_1 values ± the standard error of the mean. ^{1}H NMR spectra were performed on a Bruker 350 MHz spectrometer in D_2O.

2.5. Measurement of T1 in air, oxygen, and argon saturated water

Spin-lattice relaxation time was measured in capped test tubes containing water saturated either with air, oxygen, or argon (three

samples each for air, oxygen, and argon saturated water; nine samples in total) initially (step 0 in Fig. 1) and following systematic exposure to the atmosphere in 6 steps; each step consisting of a 5 min tube uncapping allowing for step-wise re-equilibration with atmospheric air prior to T_1 acquisition. For each sample, 15 mL of water was taken from storage bottles and added to a 15 mL polypropylene graduated conical test tube fitted with a screw tight cap. Temperature, pH and concentration of dissolved oxygen (in ppm) were measured with an Elmetron multimode CPR-411. The three 15 mL air saturated water samples were measured as taken from storage bottles without further treatment. Water samples were bubbled with either 99% oxygen (3 samples) or 99% argon gas (3 samples) at a rate of 0.1 L min^{-1} until ppm readings stabilized at a maximum of 28 ppm O_2 for oxygen addition and 0.0 ppm O_2 for addition of argon. Stabilization of ppm readings occurred after 20 min of gas bubbling for both gases. The temperature of the samples was 21.0 ± 0.5 °C at pH = 6.3. The nine samples were capped, stored upright in a Styrofoam holder and placed into the scanner for an initial T_1 measurement. Spin-lattice relation time was then measured in the series of steps previously described. Each T_1 measurement had an acquisition time of 3 h.

2.6. Measurement of oxygen consumption during photooxidation using a dissolved oxygen meter

Dissolved oxygen concentration (in ppm) was measured as a function of time during Rose Bengal (RB) sensitized photooxidation of DL-methionine, **1** (Scheme 1), at concentrations of 0.0012 M and 0.0022 M using an Elmetron multimode CPR-411 dissolved oxygen meter. Four samples were prepared by adding **1** and RB to 15 mL of air saturated water in uncapped polypropylene graduated conical test tubes. Three of the 15 mL water samples were prepared by adding 0.0027 g of **1** (MW = 149.21 g mol^{-1}) and one was prepared by addition of 0.05 g of **1** giving concentrations of 0.0012 M and 0.022 M respectively. To each of the four samples, 25 μL of a 1.5×10^{-3} M stock solution of RB was added (2.5×10^{-6} M RB). Dissolved oxygen concentration, temperature and pH were measured prior to illumination. The sample was placed in an pyrex glass beaker water bath and the dissolved oxygen meter probe was inserted into the solution which was then illuminated with light from a 400 W halogen bulb (Diall R7S Linear halogen light bulb 400 W, Diall company S.R.O., Czech Republic) through a 12 M $NaNO_2$ 385 nm cutoff filter solution until a stable reading of 0.0 ppm was measured. For two of the samples, the dissolved oxygen probe was kept in solution post-illumination to detect diffusion of atmospheric air into the oxygen-depleted solution.

2.7. Measurement of DL-methionine sulfoxide formation by ^{1}H NMR

To ensure that DL-methionine sulfoxide, **2**, is cleanly formed during photooxidation of **1**, and to correlate oxygen consumed with formation of **2**, a RB photosensitized oxidation (0.022 M **1**, 2.5×10^{-6} M RB in D_2O) was monitored by ^{1}H NMR after 100, 200, 300, 400 and 1000s of irradiation with a 400 W halogen bulb through a 12 M $NaNO_2$ 385 nm cutoff filter solution (^{1}H NMR spectra are provided in Supporting Information). The extent of Rose Bengal photobleaching was not measured; the conversion of **1** to **2** increased with time (3% conversion at 100 s to 30% conversion at 1000s by ^{1}H NMR) indicating that any decomposition of Rose Bengal had a negligible effect on oxygen consumption over these time intervals (Figure S7 in Supporting Information).

2.8. Measurement of T_1 prior to and after photooxidation of methionine in air-saturated water by MRI

Spin-lattice relaxation time T_1 was measured prior to and after 5 and 10 min of illumination of solutions containing RB and **1** in air-saturated water by MRI. Three capped test tubes containing air saturated water (control), and three air saturated water solutions containing 0.0012 M **1** and 2.5×10^{-6} M RB were prepared and stored upright in a Styrofoam holder and placed into the scanner for an initial, pre-illumination T_1 measurement. The samples were then placed together in a Pyrex glass beaker water bath. The samples were illuminated with light from a 400 W halogen bulb through a 12 M $NaNO_2$ 385 nm cutoff filter solution for 5 min after which they were placed in the scanner for measurement of T_1. After acquisition, the samples were illuminated for an additional 5 min after which they were returned to the scanner for a second T_1 measurement. A final post-illumination measurement was acquired after keeping the sample in the dark and open to the atmosphere.

2.9. Measurement of T_1 in excised normal and cancerous tissue by MRI

Once received, freshly excised samples of normal and cancerous laryngeal tissue and thyroid tissue were stored in 15 mL of deionized water in 15 mL polypropylene graduated conical test tubes fitted with a screw tight cap at 5 °C. The volume of tissues examined was ca. 4 × 4 × 4 mm (6.4×10^{-5} L) for normal and cancerous laryngeal tissue and ca. 10 × 10 × 15 mm (1.5×10^{-3} L) for normal and cancerous thyroid gland tissue. Six T_1 measurements in both superficial and deep ROI were carried out in 6 steps (steps a–f are also described in Table 1). In the first step (step a), the freshly excised tissues were placed in water and an initial T_1 was acquired. In the second step (step b), RB was to allowed to absorb into tissue samples standing in water. For normal and cancerous laryngeal tissue, 25 μL of 1.5×10^{-3} M RB was added; for normal and cancerous thyroid tissue, 100 μL of 1.5×10^{-3} M RB was added. Absorption occurred after 6 days as the aqueous solution slowly turned from red to clear, and the tissues took on reddish color. A test sample of laryngeal tissue was sliced in half post RB absorption revealing an apparently even distribution of RB throughout the tissue. Although, we cannot state the absolute concentrations of RB in tissue, the concentration did not exceed 5.8×10^{-4} M in laryngeal tissue or 1×10^{-4} M in thyroid tissue. In the third step, RB infused tissue was washed with deionized water and placed back into capped tubes containing 15 mL of fresh deionized water. Oxygen gas was then bubbled into the tissue-in-water samples at a rate of 0.1 L min^{-1} until a value of 28 ppm was recorded (20 min). The samples were capped and allowed to stand in the dark for 2 days in 28 ppm O_2 prior to T_1 acquisition (step c). Two days following the step c T_1 acquisition, a pre-illumination T_1 was acquired (step d). At this point, the tissue-in-water samples were no longer charged with oxygen gas. Samples were then placed in a Pyrex glass beaker and illuminated with light from a 400 W halogen bulb through a 12 M $NaNO_2$ 385 nm cutoff filter solution for 20 min after which they were placed in the scanner for measurement of T_1 (step e). After T_1 acquisition, the samples were illuminated for an additional 20 min after which they were returned to the scanner for a final T_1 measurement (step f). Spin lattice relaxation was also measured in samples of normal and cancerous laryngeal tissue after 20 and 40 min of illumination that were not treated with RB or oxygen charged (steps g–i). Please remove Table 1 from here and move to section 3.4

3. Results and discussion

3.1. Spin lattice relaxation time in air, oxygen, and argon-saturated water

A graph of T_1 in air, oxygen, and argon saturated water where data points 1–6 represent 6 uncapping and atmospheric air re-equilibration steps is shown in Fig. 1. The measured T_1 values in air saturated water (6 ppm oxygen) remained essentially constant throughout steps 0–7 at 3186 ms and served as a baseline. For oxygen saturated water (28 ppm O_2), the initial (step 0) T_1 was measured to be 2138 ± 62 ms with a final value of 3110 ± 54 ms at step 7, indicating loss of oxygen and air re-equilibration. An initial measurement of argon saturated water (step 0) gave a T_1 of 3771 ± 35 ms at 0 ppm O_2, and subsequent uncapping steps 1–6 allowing for argon loss and air re-equilibration leading to a final T_1 of 3189 ± 31 ms at step 7. It is clear from the data that T_1 for both argon–saturated and oxygen–saturated water converge to air-saturated T_1 after six air re-equilibration steps. Spin lattice relaxation

times for steps 0–6 are listed in Table S1 (supporting information).

Of note, our measured T_1 values for oxygen-free water at 21 °C (ca. 3800 ms) are about 20% larger than those previously reported in the literature. For comparison, a linear relationship between longitudinal relaxation time ($1/T_1$) at 26 °C ($1/T_1 = 0.284 + 4.55 \times 10^{-19} N_0$, where N_0 = the number of oxygen molecules per cm^3) reported by Hausser and Noack, gives a T_1 of 3520 ms in oxygen-free water [15]. Krynicki, who also carefully measured T_1 in oxygen-free water as a function of temperature reported values of 3150 ms and 3570 ms at 20 °C and 25 °C respectively [17]. In this work, our obtained value for argon–saturated water (T_1 = 3771 ± 35 ms at ~ 0 ppm O_2) agrees with our photooxidation experiments where complete photoconsumption of measurable oxygen in the same volume of water (15 mL) at the same temperature (21 °C) gave T_1 times between 3772 ms and 3817 ms (Table S3 in supporting information).

3.2. Measurement of oxygen consumption during photooxidation of methionine in air-saturated water using a dissolved oxygen meter

Time required to deplete oxygen in 15.0 mL of air-saturated water during RB photosensitized oxidation of **1** is shown in Fig. 2. For 0.0012 M **1**, the measurable available oxygen in air saturated water (6.5 ppm ~ 3×10^{-6} mol O_2 in 15.0 mL of water) was photoconsumed within 300 s of illumination corresponding to a 33% conversion of **1** using the stoichiometry in Scheme 1 (**1** + $^1O_2 \rightarrow$ 2(**2**)). Illumination of 0.022 M **1** photoconsumed available oxygen (8 ppm ~ 3.75×10^{-6} mol O_2 in 15.0 mL of water) within 100 s (2% conversion of **1**). Methionine was found to trap $^1O_2$ to form **2** cleanly without detectable formation of N–S cycloaddition products which liberate H_2O_2 and can begin to compete with S-oxidation at pH > 6 [45].

Our water solutions had a pH of 6.3 and between 100 s and 1000s of illumination, only **2** was detected in identically performed reactions by ^1H NMR in D_2O (Supporting Information). In D_2O, the percent conversion of **1** to **2** after a 100 s illumination of 0.022 M **1** and 2.5×10^{-6} M RB was 6%. The larger percent conversion (5.6% vs 2.5%) at 100 s of illumination time reflects the longer lifetime of $^1O_2$ in D_2O (3.1 μs in H_2O vs 65 μs in D_2O) [45,46].

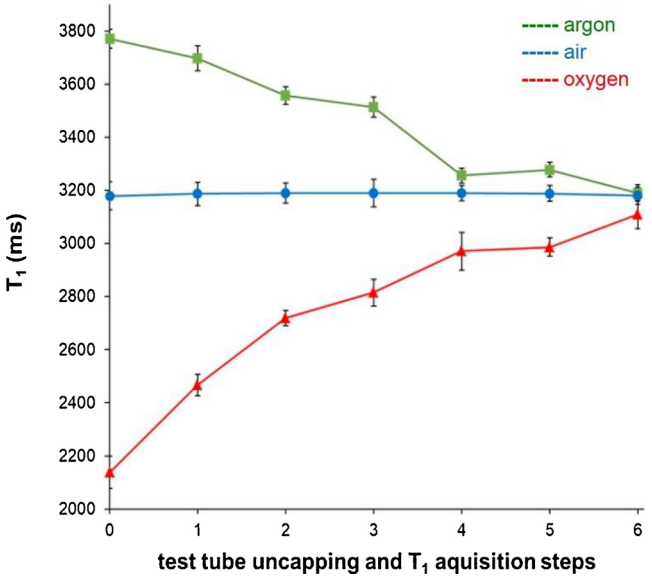

Fig. 1. Spin-lattice relaxation time, T_1 (in milliseconds), measured in a series of seven steps for 15.0 mL of air-saturated (blue circles), argon–saturated (green squares) and oxygen–saturated (red triangles) water. Step 0 is the initial T_1 measurement. Six T_1 measurements were acquired after each sequential step consisting of a 5 min of exposure to atmospheric air (test tube uncapping), tube recapping and a 3 h T_1 acquisition time. Each point is an average of three measurements reported as average ± SEM.

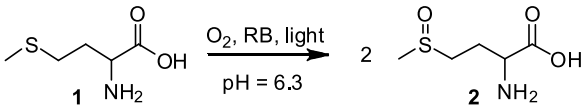

Scheme 1. Photooxidation of DL-methionine.

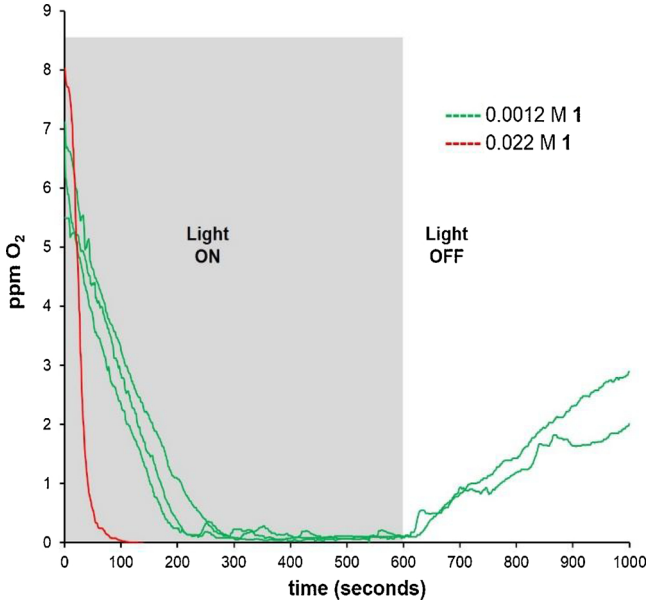

Fig. 2. Dissolved oxygen concentration (in ppm) measured with an Elmetron multimode CPR-411 dissolved oxygen meter as a function of time (in seconds) during illumination of 15.0 mL air-saturated aqueous samples of RB (2.5×10^{-6} M) and either 0.0012 M **1** (green curves) or 0.022 M **1** (red curve) in air saturated water. In two experiments (green curves), ppm O_2 was measured for an additional 400 s post-illumination to record atmospheric air re-equilibration.

3.3. Measurement of T_1 prior to and after photooxidation of methionine in air-saturated water by MRI

The spin-lattice relaxation time T_1 of water increased by 492 ± 53 ms during 300 s of illumination of solutions containing 0.0012 M **1** and 2.5×10^{-6} M RB in air-saturated water as shown graphically in Fig. 3. Samples of air saturated water (15 mL) containing 6.5 ppm (~ 3×10^{-6} mol) O_2 that were measured concurrently with solutions containing **1** and RB, remained essentially constant at a T_1 value of 3266 ms throughout the experiment. Post-illumination T_1 values in water containing **1** and RB that were uncapped and left in the dark, returned to air saturated values (Fig. 3). As in the case of identical reactions measured with a dissolved oxygen meter described in the last section, measurable oxygen was photoconsumed within 300 s of illumination (from 0 to 300 s and from start[a] to 900 s); T_1 measurements after 300 s (at 600 s and 1200s) were essentially unchanged indicating that dissolved oxygen within the sample was already photoconsumed and conversion of **1** to **2** had reached a maximum. Again, using the stoichiometry in Scheme 1 (**1** + $^1O_2 \rightarrow$ 2(**2**)), photoconsumption of 3×10^{-6} mol O_2 in 300 s corresponds to 33% conversion of **1** to **2**. Air re-equilibration followed by a second round of illumination for 300 s (start[a] to 900 s) led to consumption of an additional 3×10^{-6} mol O_2 and a 66% conversion of **1** at 900 and 1200s.

3.4. Measurement of T_1 in excised healthy and cancerous laryngeal tissue by MRI

Measured values of superficial and deep T_1 in excised tissue after a series of experimental steps a–f (g–i for untreated laryngeal tissue) are

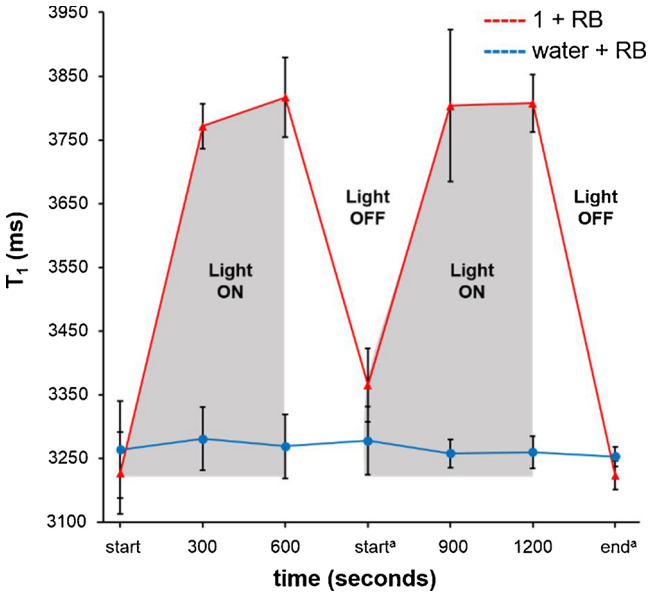

Fig. 3. Spin-lattice relaxation time, T_1, measured after 300, 600, 900 and 1200 s of illumination of 15.0 mL aqueous samples of 0.0012 M **1** and RB (2.5×10^{-6} M) (red triangles) in air saturated water. An initial T_1 value (start) was acquired prior to illumination. a. Start[a] and end[a] represent T_1 measurements acquired post-illumination after 9 h of air exposure in the dark. Measurements are an average of 3 individual experiments and error bars represent average $T_1 \pm$ SEM. Blue circles represent simultaneous T_1 measurements of 15.0 mL of air saturated water, also presented graphically as $T_1 \pm$ SEM.

presented in Table 1. Superficial and deep ROI were chosen to determine potential differences in T_1 due to changes in tissue water and dissolved oxygen after preparative steps and after illumination. In tissue samples, superficial and deep ROI T_1 are reported as an average of 4 separate slice T_1 values ± the standard error of the mean. The tissue samples were subjected to preparative steps 24 h after excision and were presumed to be metabolically inactive, necrotic tissue when received. A photograph of Rose Bengal infused cancerous thyroid tissue and the corresponding T_2-weighted imgage with superficial and deep regions delineated is shown in Fig. 4. In each tissue measurement, T_1 (superficial) > T_1 (deep) presumably due to differences in tissue integrity, water and oxygen content [32].

An increase in tissue water content was apparent as an increase in T_1 was observed after RB absorption (between steps a and b), where the tissues were allowed to stand in 15 mL of either 2.5×10^{-6} M RB (cancerous and normal laryngeal tissue) or 1.0×10^{-5} M RB (cancerous and normal thyroid tissue) solution. After the six day RB absorption step, superficial and deep T_1 in cancerous laryngeal tissue increased by 708 ms and 468 ms respectively. A similar trend occurred in normal laryngeal tissue (ΔT_1 superficial = 761 ms, ΔT_1 deep = 795 ms). The same trend was found in cancerous and normal thyroid tissue to a lesser extent. We attribute this increase in both superficial and deep T_1 to an increase in free interstitial water and tissue denaturation as a result of the prolonged RB absorption. The increase in T_1 was not due to addition of RB as shown in control experiments. Oxygenation of the RB infused tissue (step c) showed a remarkable decrease in T_1 in both cancerous and normal laryngeal and thyroid tissue. Placing tissue samples in 15 mL of water at 28 ppm O_2 for 48 h decreased both superficial and deep T_1 by 740 ms (averaged over all tissues). Two days following step c (oxygen charge), tissue sample tubes were uncapped and exposed to air for re-equilibration and a pre-illumination T_1 was acquired (step d). At this point, the tissue-in-water samples were no longer charged with oxygen gas and pre-illumination T_1 increased substantially from the previous (oxygen charged) measurements indicating both oxygen loss and an additional increase in interstitial water. The next T_1 measurements were acquired after 20 and 40 min of illumination of the

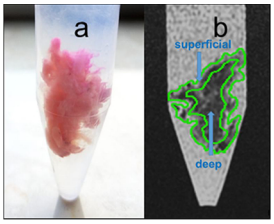

Fig. 4. a) Representative photograph of Rose Bengal infused tissue (thyroid neoplasm) and b) the corresponding T_2 weighted imgage with superficial and deep regions delineated.

Rose Bengal infused tissues in 15 mL of water with a 400 W halogen bulb through a 12 M $NaNO_2$ 385 nm cutoff filter solution. We observed no change that would indicate oxygen photoconsumption in the superficial and deep T_1 of cancerous laryngeal tissue after 20 min of illumination. However, a notable percent increase in T_1 was observed in normal laryngeal tissue (15% superficial and 18% deep), cancerous thyroid tissue (11% superficial and 9.4% deep), and in normal thyroid tissue (6.7% superficial and 11% deep). No percent increases in superficial or deep T_1 were observed for any of the tissue samples examined after 40 min of illumination which suggests that the increase in T_1 observed after 20 min of illumination in normal laryngeal tissue and in cancerous and normal thyroid tissue is not due to water uptake, but rather oxygen depletion as a result of photodynamic action.

4. Conclusions

Direct T_1 endogenous oxygen contrast MRI can be implemented to monitor oxygen photoconsumption *in vitro*. The proton spin-lattice relaxation time of water gradually decreased in argon saturated aqueous solutions that were exposed to atmospheric air allowing for oxygen re-equilibration. Likewise, an increase in T_1 was measured following exposure of oxygen saturated water to air. This well-known and verified dependence of T_1 on dissolved aqueous oxygen was demonstrated here in systems undergoing oxygen photoconsumption. Proton spin-lattice relaxation time increased in samples consisting either aqueous solutions or excised tissue that contained RB, dissolved oxygen and substances capable of trapping singlet oxygen during illumination. In aqueous solutions containing RB and methionine, T_1 measurements of oxygen photoconsumption are straightforward and easily rationalized. Proton spin-lattice relaxation time of water increases due to irreversible singlet oxygen trapping, and the time required to essentially deplete dissolved oxygen as measured by MRI corresponds with measurements performed with a dissolved oxygen meter. It should be noted that the increases in T_1 observed following the photooxidation of **1** and irradiation of RB-infused tissue only reflects bulk consumption of dissolved triplet oxygen. We are assuming that the consumption of dissolved triplet oxygen results from its conversion to the singlet state which is ultimately trapped.

Results obtained in experiments with excised tissue are less easily explained mainly due to the fact that the substances responsible for $^1O_2$ trapping within the tissues are not specified here, and tissue was allowed to stand in water up to 6 days between T_1 acquisitions during RB absorption and after oxygen loading which led to water uptake. Consistent trends in T_1 measured during tissue sample preparation and illumination yield four main conclusions: (1) T_1 of all laryngeal and thyroid tissue measured both superficially and deep increases during RB absorption due to water uptake; RB itself was found to have no effect on T_1 and is not acting as a contrast agent, (2) decreases in T_1 measured both superficially and deep indicate that interstitial oxygen concentration in tissue samples increases during their suspension in oxygen saturated water. After 2 days post-oxygenation during which time tissue was suspended in air-saturated water, T_1 again increased due to oxygen loss and water uptake, (3) in most cases, a positive percent increase in T_1 was observed between an initial pre-illumination acquisition and

Table 1
Spin-lattice relaxation time in excised tissue.

	T_1 (ms)*			
	laryngeal neoplasm		**normal laryngeal tissue**	
	superficial	*deep*	*superficial*	*deep*
	2295 ± 96[a]	1708 ± 57[a]	2171 ± 32[a]	1708 ± 57[a]
	3003 ± 384[b]	2176 ± 431[b]	2932 ± 159[b]	2503 ± 342[b]
	2129 ± 39[c]	1663 ± 41[c]	2167 ± 14[c]	1640 ± 148[c]
0 min hυ	3548 ± 107[d]	2985 ± 55[d]	3463 ± 148[d]	2546 ± 132[d]
20 min hυ	3680 ± 127[e]	3038 ± 200 [e]	3976 ± 120[e]	3009 ± 96 [e]
T_1 percent increase from 0 to 20 min hυ	3.7%	1.8%	15%	18%
40 min hυ	3741 ± 35[f]	3061 ± 142[f]	3891 ± 30[f]	3001 ± 55[f]
T_1 percent increase from 20 to 40 min hυ	1.7%	0.8%	−2.6%	−0.3%
	thyroid neoplasm		**normal thyroid tissue**	
	superficial	*deep*	*superficial*	*deep*
	2626 ± 48[a]	2114 ± 92[a]	2223 ± 47[a]	1647 ± 53[a]
	2751 ± 56[b]	2532 ± 59[b]	2529 ± 75[b]	2009 ± 79[b]
	1953 ± 67[c]	1523 ± 44[c]	1995 ± 64[c]	1442 ± 132[c]
0 min hυ	3013 ± 103[d]	2449 ± 62[d]	3001 ± 85[d]	2277 ± 75[d]
20 min hυ	3351 ± 124[e]	2680 ± 156 [e]	3201 ± 123[e]	2518 ± 140[e]
T_1 percent increase from 0 to 20 min hυ	11%	9.4%	6.7%	11%
40 min hυ	3441 ± 27[f]	2656 ± 92[f]	3145 ± 134 [f]	2656 ± 92[f]
T_1 percent increase from 20 to 40 min hυ	2.7	−0.9	−1.7	5.5
	laryngeal neoplasm (illlumination without rose bengal)		**normal laryngeal tissue (illumination without rose bengal)**	
	superficial	*deep*	*superficial*	*deep*
0 min hυ	2484 ± 35[g]	1638 ± 48[g]	2372 ± 132 [g]	1463 ± 78[g]
20 min hυ	2398 ± 102[h]	1633 ± 96[h]	2347 ± 121 [h]	1436 ± 156[h]
T_1 percent increase from 0 to 20 min	−3.5%	−0.3%	−1.1%	−1.8%
40 min hυ	2392 ± 81[i]	1689 ± 39[i]	2052 ± 176 [i]	1411 ± 159[i]
T_1 percent increase from 20 to 40 min hυ	−0.2%	3.4%	−12%	−1.7%

[a] Initial T_1 measurement.
[b] Measurement after 6 days of Rose Bengal absorption.
[c] Measurement after 6 days of rose bengal absorption and 48 h standing in oxygen saturated water.
[d] Initial T_1 measurement prior to illumination.
[e] T_1 after 20 min illumination.
[f] T_1 after 40 min illumination.
[g] Initial T_1 (no Rose Bengal).
[h] 20 min illumination (no Rose Bengal).
[i] 40 min of illumination (no Rose Bengal).
* Superficial and deep ROI T_1 are reported as an average of 4 separate (1 mm) slice T_1 values ± the standard error of the mean.

after 20 min of illumination of RB infused tissue. We conclude that the tendency of T_1 to increase after 20 min of illumination is due to oxygen photoconsumption and not to water uptake or other influence elicited by tissue illumination. This conclusion is proposed since with one exception a positive percent increase in T_1 was not observed to occur after 40 min of illumination nor was a positive percent increase in T_1 observed after a 20 min illumination of tissue in the absence of RB.

Appendix A. Supplementary data

Supplementary material related to this article can be found, in the online version, at doi:https://doi.org/10.1016/j.pdpdt.2019.02.007.

References

[1] D.E. Dolmans, D. Fukumura, R.K. Jain, Photodynamic therapy for Cancer, Nat. Rev. Cancer 3 (5) (2003) 380–387.
[2] U. Schmidt-Erfurth, T. Hasan, Mechanisms of action of photodynamic therapy with verteporfin for the treatment of age-related macular degeneration, Surv. Ophthalmol. 45 (3) (2000) 195–214.
[3] A.E. O'Conner, W.M. Gallagher, A.T. Byrne, Porphyrin and nonporphyrin photosensitizers in oncology: preclinical and clinical advances in photodynamic therapy, Photochem. Photobiol. 85 (5) (2009) 1053–1074.
[4] M.R. Hamblin, T. Hasan, Photodynamic therapy: a new antimicrobial approach to infectious disease? Photochem. Photobiol. Sci. 3 (2004) 436–450.
[5] R. Rossi, N. Bruscino, F. Ricceri, M. Grazzini, M. Dindelli, T. Lotti, Photodynamic treatment for viral infections of the skin, G. Ital. Dermatol. Venereol. 144 (1) (2009) 79–83.
[6] A.P. Castano, T.N. Demidova, M.R. Hamblin, Mechanisms in photodynamic therapy: part one-photosensitizers, photochemistry and cellular localization, Photodiagnosis Photodyn. Ther. 1 (4) (2004) 279–293.
[7] C.S. Foote, Mechanisms of photosensitized oxidation, Science 162 (1968) 963–970.
[8] L. Gray, A. Conger, M. Ebert, S. Hornsey, O. Scott, The concentration of oxygen dissolved in tissues at time of irradiation as a factor in radiotherapy, Br. J. Radiol. 26 (312) (1953) 638–648.
[9] B.J. Tromberg, A. Orenstein, S. Kimel, S.J. Barker, J. Hyatt, J.S. Nelson, M.W. Berns, In vivo tumor oxygen tension measurements for the evaluation of the efficiency of photodynamic therapy, Photochem. Photobiol. 52 (2) (1990) 375–385.
[10] J. Zilberstein, A. Bromberg, A. Frantz, V. Rosenbach-Belkin, A. Kritzmann, R. Pfefermann, Y. Salomon, A. Scherz, Light-dependent oxygen consumption in bacteriochlorophyll-serine-treated melanoma tumors: on-line determination using a tissue-inserted oxygen microsensor, Photochem. Photobiol. 65 (6) (1997) 1012–1019.
[11] J.H. Woodhams, A.J. Macrobert, S.G. Bown, The role of oxygen monitoring during photodynamic therapy and its potential for treatment dosimetry, Photochem. Photobiol. Sci. 6 (12) (2007) 1246–1256.
[12] J. Pacheco-Torres, P. López-Larrubia, P. Ballesteros, S. Cerdán, Imaging tumor hypoxia by magnetic resonance methods, NMR Biomed. 24 (1) (2011) 1–16.
[13] N. Bloembergen, E.M. Purcell, R.V. Pound, Relaxation effects in nuclear magnetic resonance absorption, Phys. Rev. 73 (7) (1948) 679–712.
[14] L. Guilotto, Arch. Sci. (Facicule Specjale) 9 (1956) 212.
[15] R. Hausser, F. Noack, Kernmagnetische relaxation und korrelation im system Wasser- sauerstoff, Z. Naturforsch. A 20 (12) (1965) 1668–1675.
[16] M.E. Mirhej, Proton spin relaxation by paramagnetic molecular oxygen, Can. J. Chem. 43 (5) (1965) 1130–1138.
[17] K. Krynicki, Proton spin-lattice relaxation in pure water between 0°C and 100°C, Physica 32 (1) (1966) 167–178.
[18] J. Glasel, The physics and physical chemistry of water, in: F. Franks (Ed.), Water, A Comprehensive Treatise, vol. 1, Plenum Press, New York, 1972, pp. 235–236.
[19] S.F. Akber, Correlation between oxygen tension and spin-lattice relaxation rate in tumors, Eur. J. Radiol. 9 (1) (1989) 56–59.
[20] B.A. Berkowitz, Role of dissolved plasma oxygen in hyperoxia-induced contrast, Magn. Reson. Imaging 15 (1) (1997) 123–126.
[21] S. Ogawa, T.M. Lee, A.R. Kay, D.W. Tank, Brain magnetic resonance imaging with contrast dependent on blood oxygenation, Proc. Natl. Acad. Sci. U. S. A. 87 (24) (1990) 9868–9872.
[22] S. Gross, A. Gilead, A. Scherz, M. Neeman, Y. Salomon, Monitoring photodynamic therapy of solid tumors online by bold-contrast MRI, Nat. Med. 9 (10) (2003) 1327–1331.

[23] K. Matsumoto, M. Bernardo, S. Subramanian, P. Choyke, J.B. Mitchell, M.C. Krishna, M.J. Lizak, MR assessment of changes of tumor in response to hyperbaric oxygen treatment, Magn. Reson. Med. 56 (2) (2006) 240–246.
[24] G. Zaharchuk, R.F. Busse, G. Rosenthal, G.T. Manley, O.A. Glenn, W.P. Dillon, Noninvasive oxygen partial pressure measurement of human body fluids in vivo using magnetic resonance imaging, Acad. Radiol. 13 (8) (2006) 1016–1024.
[25] V.A. Bourke, D. Zhao, J. Gilio, C.H. Chang, L. Jiang, E.W. Hahn, R.P. Mason, Correlation of radiation response with tumor oxygenation in the dunning prostate R3327-AT1 tumor, Int. J. Radiat. Oncol. Biol. Phys. 67 (4) (2007) 1179–1186.
[26] J. Pacheco-Torres, D. Zhao, A. Contero, R.P. Mason, Differential physiological response to carbogen of two diverse prostate tumor lines detected by tissue water ^{1}H MRI, Proceedings of the 16th Annual Meeting ISMRM (2008) 4337.
[27] J.P. O'Connor, J.H. Naish, G.J. Parker, J.C. Waterton, Y. Watson, G.C. Jayson, G.A. Buonaccorsi, S. Cheung, D.L. Buckley, D.M. McGrath, C.M. West, S.E. Davidson, C. Roberts, S.J. Mills, C.L. Mitchell, L. Hope, N.C. Ton, A. Jackson, Preliminary study of oxygen-enhanced longitudinal relaxation in MRI: a potential novel biomarker of oxygenation changes in solid tumors, Int. J. Radiat. Oncol. Biol. Phys. 75 (4) (2009) 1209–1215.
[28] Y. Ding, R.P. Mason, R.W. McColl, Q. Yuan, R.R. Hallac, R.D. Sims, P.T. Weatherall, Simultaneous measurement of tissue oxygen level-dependent (TOLD) and blood oxygenation level-dependent (BOLD) effects in abdominal tissue oxygenation level studies, J. Magn. Reson. Imaging 38 (5) (2013) 1230–1236.
[29] R.R. Hallac, H. Zhou, R. Pidikiti, K. Song, S. Stojadinovic, D. Zhao, T. Solberg, P. Peschke, R.P. Mason, Correlations of noninvasive bold and told MRI with pO_2 and relevance to tumor radiation response, Magn. Reson. Med. 71 (5) (2014) 1863–1873.
[30] D. Zhao, J. Pacheco-Torres, R.R. Hallac, D. White, P. Peschke, S. Cerdán, R.P. Mason, Dynamic oxygen challenge evaluated by NMR T_1 and T_2*–Insights into tumor oxygenation, NMR Biomed. 28 (8) (2015) 937–947.
[31] R.W. Tain, A.M. Scotti, W. Li, X.J. Zhou, K. Cai, Imaging short-lived reactive oxygen species (ROS) with endogenous contrast MRI, J. Magn. Reson. Imaging 47 (1) (2018) 222–229.
[32] Y.H. Liu, R.M. Hawk, S. Ramaprasad, In vivo relaxation time measurements on a murine tumor model-prolongation of T_1 after photodynamic therapy, Magn. Reson. Imaging 13 (2) (1995) 251–258.
[33] K.G. Helmer, S. Han, C.H. Sotak, On the correlation between the water diffusion coefficient and oxygen tension in RIF-1 tumors, NMR Biomed. 11 (3) (1998) 120–12130.
[34] V. Plaks, N. Koudinova, U. Nevo, J.H. Pinthus, H. Kanety, Z. Eshhar, J. Ramon, A. Scherz, M. Neeman, Y. Salomon, Photodynamic therapy of established prostatic adenocarcinoma with TOOKAD: a biphasic apparent diffusion coefficient change as potential early MRI response marker, Neoplasia 6 (3) (2004) 224–233.
[35] Z. Huang, M.A. Haider, S. Kraft, Q. Chen, D. Blanc, B.C. Wilson, F.W. Hetzel, Magnetic resonance imaging correlated with the histopathological effect of Pd-Bacteriopheophorbide (Tookad) photodynamic therapy on the normal canine prostate gland, Lasers Surg. Med. 38 (7) (2006) 672–681.
[36] B. Fei, H. Wang, J.D. Meyers, D.K. Feyes, N.L. Oleinick, J.L. Duerk, High-field magnetic resonance imaging of the response of human prostate Cancer to pc 4-Based photodynamic therapy in an animal model, Lasers Surg. Med. 39 (9) (2007) 723–730.
[37] H. Wang, B. Fei, Diffusion-weighted MRI for monitoring tumor response to photodynamic therapy, J. Magn. Reson. Imaging 32 (2) (2010) 409–417.
[38] M. Sajisevi, N.R. Rigual, D.A. Bellnier, M. Seshadri, Image-guided interstitial photodynamic therapy for squamous cell carcinomas: preclinical investigation, J. Oral Maxillofac. Surg. Med. Pathol. 27 (2) (2015) 159–165.
[39] T.J. Schreurs, S.J. Hectors, I. Jacobs, H. Grüll, K. Nicolay, G.J. Strijkers, Quantitative multi-parametric magnetic resonance imaging of tumor response to photodynamic therapy, PLoS One 11 (11) (2016) e0165759.
[40] M. Toussaint, S. Pinel, F. Auger, N. Durieux, M. Thomassin, E. Thomas, A. Moussaron, D. Meng, F. Plénat, M. Amouroux, T. Bastogne, C. Frochot, O. Tillement, F. Lux, M. Barberi-Heyob, Proton MR spectroscopy and diffusion MR imaging monitoring to predict tumor response to interstitial photodynamic therapy for glioblastoma, Theranostics 7 (2) (2017) 436–451.
[41] R. Damadian, Tumor detection by nuclear magnetic resonance, Science 171 (3976) (1971) 1151–1153.
[42] C. Schweitzer, R. Schmidt, Physical mechanisms of generation and deactivation of singlet oxygen, Chem. Rev. 103 (2003) 1685–1758.
[43] J. Moan, K. Berg, The photodegradation of porphyrins in cells can be used to estimate the lifetime of singlet oxygen, Photochem. Photobiol. 53 (4) (1991) 549–553.
[44] S. Hatz, J.D. Lambert, P.R. Ogilby, Measuring the lifetime of singlet oxygen in a single cell: addressing the issue of cell viability, Photochem. Photobiol. Sci. 6 (2007) 1106–1116.
[45] P.K. Sysak, C.S. Foote, T.-Y. Ching, Chemistry of singlet oxygen-XXV. Photooxygenation of methionine, Photochem. Photobiol. 26 (1977) 19–27.
[46] P.R. Ogilby, C.S. Foote, Chemistry of Singlet Oxygen. 42. Effect of Solvent, Solvent Isotopic Substitution, and Temperature on the Lifetime of Singlet Molecular Oxygen ($^{1}\Delta_g$), J. Am. Chem. Soc. 104 (1982) 2069–2070.